Free Radical Research

ISSN: (Print) (Online) Journal homepage: https://www.tandfonline.com/loi/ifra20

Heavy-ion beam-induced reactive oxygen species and redox reactions

Ken-ichiro Matsumoto, Megumi Ueno, Yoshimi Shoji & Ikuo Nakanishi

To cite this article: Ken-ichiro Matsumoto, Megumi Ueno, Yoshimi Shoji & Ikuo Nakanishi (2021) Heavy-ion beam-induced reactive oxygen species and redox reactions, Free Radical Research, 55:4, 450-460, DOI: 10.1080/10715762.2021.1899171

To link to this article: https://doi.org/10.1080/10715762.2021.1899171

Published online: 17 Mar 2021.

FREE RADICAL RESEARCH
2021, VOL. 55, NO. 4, 450–460
https://doi.org/10.1080/10715762.2021.1899171

Taylor & Francis
Taylor & Francis Group

REVIEW ARTICLE

Heavy-ion beam-induced reactive oxygen species and redox reactions

Ken-ichiro Matsumoto, Megumi Ueno, Yoshimi Shoji and Ikuo Nakanishi

Quantitative RedOx Sensing Group, Department of Basic Medical Sciences for Radiation Damages, National Institute of Radiological Sciences, Quantum Medical Science Directorate, National Institutes for Quantum and Radiological Science and Technology, Chiba, Japan

ABSTRACT

Quantification and local density estimation of radiation-induced reactive oxygen species (ROS) were described focusing on our recent and related studies. Charged particle radiation, i.e. heavy-ion beams, are currently utilized for medical treatment. Differences in ROS generation properties between photon and charged particle radiation may lead to differences in the quality of radiation. Radiation-induced generation of ROS in water was quantified using several different approaches to electron paramagnetic resonance (EPR) techniques. Two different densities of localized hydroxyl radical (•OH) generation, i.e. milli-molar and molar levels, were described. Yields of sparse •OH decreased with increasing linear energy transfer (LET), the yield total •OH was not affected by LET. In the high-density, molar level, •OH environment, •OH can react and directly make hydrogen peroxide (H_2O_2), and then possible to form a high-density H_2O_2 cluster. The amount of total oxidation reactions caused by oxidative ROS, such as •OH and hydroperoxyl radial ($HO_2^•$), was decreased with increasing LET. Possibilities of the sequential reactions were discussed based on the initial localized density at the generated site. Water-induced ROS have been well investigated. However, little is known about radiation-induced free radical generation in lipidic conditions. Radio-chemistry to understand the sequential radio-biological effects is still under development.

ARTICLE HISTORY
Received 9 November 2020
Revised 28 February 2021
Accepted 2 March 2021

KEYWORDS
Carbon-ion beam; reactive oxygen species; redox reaction; ionizing radiation; hydroxyl radical; hydrogen peroxide

Introduction

Radiation is a ray of particles and/or electromagnetic waves that can travel through a material bringing energy (Table 1). There is ionizing and non-ionizing radiation. Non-ionizing radiation includes electric waves, infrared, ultraviolet, etc. Ionizing radiation, which includes α-ray, β-ray, γ-ray, X-ray, neutron, heavy-ion beams, etc., can ionize or excite the molecules constituting the irradiated material objects. In general, the term "radiation" refers to ionizing radiation.

Ionizing radiation does not discriminate among molecules to interact with. However, the biological effects of radiation may exhibit specificity, such as radio-sensitivity of specific organs/tissues, tissue oxygen concentrations, and other chemical radiation modifiers. Biological effects of ionizing radiation are induced through 2 mechanisms, direct action and indirect action [1–4]. Direct action is induced by the direct ionization/excitation of a biologically important molecule by ionizing radiation. Indirect action is induced from a chemical reaction of reactive species, such as reactive oxygen species (ROS) or other free radical species, caused by water radiolysis with a biological molecule. As water constitutes approximately 70% of living organisms, ionizing radiation interacts with water molecules at a higher rate than other molecules. It is considered that 70% of the effects of ionizing radiation are due to indirect action mediated by ROS. The indirect action mediated by ROS or other chemical species provides an opportunity to regulate its reaction.

X-rays and γ-rays are electromagnetic radiation with wave and particle (photon) duality. Electromagnetic waves or non-charged particles with no mass have little interaction with other molecules. In other words, electromagnetic waves or photons have high permeability. Highly permeating photons affect not only the target, but also behind and in front of it (Figure 1(A)). In

CONTACT Ken-ichiro Matsumoto matsumoto.kenichiro@qst.go.jp Quantitative RedOx Sensing Group, Department of Basic Medical Sciences for Radiation Damages, National Institute of Radiological Sciences, Quantum Medical Science Directorate, National Institutes for Quantum and Radiological Science and Technology, 4-9-1 Anagawa, Inage-ku, Chiba 263-8555, Japan

Table 1. Classification of radiation.

Ionization	Name of Radiation	Electromagnetic wave/Particle	Charge	Source/Generation
non-ionizing	electro wave (radio wave, microwave, infrared, ultraviolet, etc.)	electromagnetic wave (photon)	0	Varies depending on wavelength.
indirectly ionizing	X-ray	electromagnetic wave (photon)	0	extranuclear interaction
(uncharged particle)	γ-ray	electromagnetic wave (photon)	0	γ nuclear disintegration
	neutron-ray	neutron	0	nuclear disintegration/nuclear spallation
directly ionizing	α-ray	He nucleus	+2	α nuclear disintegration
(charged particle)	β-ray	electron	−1	β^- nuclear disintegration
		positron	+1	β^+ nuclear disintegration
	electron-beam	electron	−1	acceleration
	pi-meson-beam	pi-meson	−1	nuclear spallation
	proton-beam	H nucleus	+1	cosmic ray/acceleration
	heavy-ion beam	nucleus heavier than H	> +2	cosmic ray/acceleration

addition, photons have relatively high oxygen effects compared with charged particle radiation, and ROS generation by photon radiation in normal tissues is considered a major problem of radiation therapies.

In contrast to photons, charged particle radiation, termed high linear energy transfer (LET) radiation, gives a relatively large amount of energy to all molecules, i.e. dense ionization/excitation, on its linear track. LET is defined as the energy transferred per unit of distance (keV/μm). Charged particle radiation has a characteristic dose and LET distribution in the irradiated sample (Figure 1(B)). LET of a charged particle will increase gradually depending on its decrease in speed in the material it is passing through, and after losing all its kinetic energy, it is stopped. This high-LET at the endpoint of the particle beam is known as the Bragg peak. Due to such dense ionization/excitation, direct effects have been considered more important for the effects of high-LET charged particle radiation. Indeed, it has a lower indirect action [5,6] and lower oxygen effect [7,8] than photon radiation. In the past 3 decades, charged particle radiation, which has a higher probability of interaction, has been utilized in cancer therapy to improve therapeutic performance.

The oxygen effects of heavy-ion beam are relatively small and are not considered problematic in the early stage of carbon-ion therapy, when relatively low-dose high-fractionated protocols were used. The generation of ROS by carbon-ion beams is no longer negligible when the clinical dose becomes higher in low-fractionated high-dose protocols. Therefore, the details of ROS generation induced by clinical carbon-ion beams must be investigated to improve carbon-ion therapy by efficiently using ROS and to prevent potentially serious side effects.

Differences in ROS generation properties between photon and particle radiation may lead to differences in the quality of radiation. Radiation-induced generation

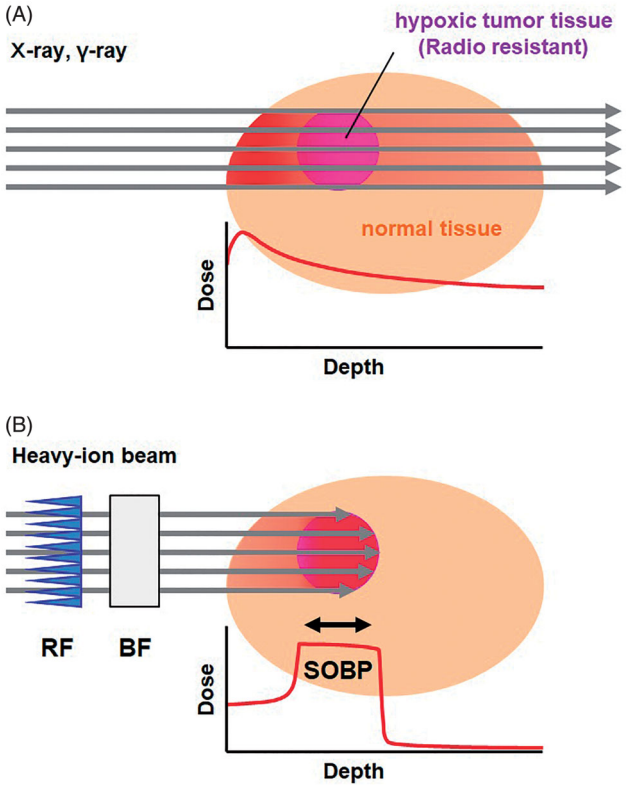

Figure 1. Difference in dose distribution between photon irradiation and heavy-ion beam irradiation. (A) Schematic drawing of the geometry of photon irradiation and dose distribution. (B) Schematic drawing of heavy-ion beam irradiation and dose distribution. The range and position of the spread-out Bragg peak (SOBP) was adjusted on the target tissue using a ridge filter (RF) and binary filter (BF). The thickness of the RF determines the SOBP thickness. The thickness of BF determines the depth of the total beam end, i.e. the SOBP can be shifted by changing the BF thickness.

of ROS has been quantified using several different approaches and the possibilities of sequential reactions were discussed based on the initial localized density at the generated site. In this review paper, our recent

reports are discussed with additional commentary and other related studies are introduced for comparison.

Generation of heavy-ion beams at medical accelerators for radiation therapy and spread of particle-beam therapy in Japan

The most well-known natural charged particle radiation is the α particle, which is a helium atomic nucleus with substantial kinetic energy that often accompanies the disintegration of an unstable nucleus of high atomic number. In general, the energy of α-rays is small and has continuous values. The direction of α-rays exiting the disintegrating nucleus is not able to be controlled. Using an accelerator, however, a radiation beam of an arbitrary atomic nucleus with an arbitrary exact energy and exact direction can be prepared, i.e. heavy-ion beams, for example carbon-ion beams are an accelerated carbon atomic nuclei. Carbon-ion beams and/or other heavy-ion beams are artificially charged particle radiation currently utilized for medical treatment.

Carbon-ion beams, a modern radiation therapy, has been utilized in medical treatment for cancer and/or other diseases [9]. A massive medical accelerator at the National Institute of Radiological Sciences (Chiba, Japan), named HIMAC (Heavy-Ion Medical Accelerator in Chiba) was built in October 1993, and carbon-ion medical treatments began from June 1994 [9]. The total number of patients treated at HIMAC was 11,834 from 1994 through March 2019 [10]. Carbon atomic nuclei can be accelerated to 70% the speed of light at HIMAC using a combination of a linear accelerator and synchrotron [11]. Downsized versions of HIMAC were built throughout Japan, and carbon-ion therapy was started from March 2010 at Gunma University Heavy Ion Medical Center [12], from August 2013 at SAGA HIMAT (SAGA Heavy-Ion Medical Accelerator in Tosu) [13], from December 2015 at i-ROCK (Ion-beam Radiation Oncology Center in Kanagawa) [14], and from October 2018 at Osaka HIMAK at Osaka Heavy Ion Therapy Center [15]. The Hyogo Ion Beam Medical Center (HIBMC) has also performed both proton-beam and carbon-ion beam therapy from 2001 [16]. There are 5 medical centers currently working on carbon-ion therapy in Japan. There are at least another 8 medical accelerators currently performing heavy-ion therapy worldwide [17].

The instruments [18,19] and protocols [20] of heavy-ion beam therapy are improving year-by-year. To alleviate the mental and physical pain of patients, hypofractionation protocols have been introduced to carbon-ion therapy, especially single-irradiation for lung cancer treatment [21]. Molecular chemical approaches to improve particle beam therapy have been less frequently conducted and reported than other physical and/or biological approaches.

Track structure of heavy-ion beams

The spur diffusion model is widely accepted as a model for explaining the initial ionizing/exciting process by ionizing radiation in water [22,23]. Initial radiolysis products in water, such as hydroxyl radical (•OH), hydrogen radical (•H), and hydrated electron (e_{aq}^-), are initially localized in the nano-meter regions called spur in picosecond range. After diffusion and intra- and/or inter-spur reactions of the species, spatially uniform distribution of products would be made during microsecond range. For low-LET radiation it is an effective model for explaining the initial ionizing products in water [22,23]. The spur model is confirmed by Monte Carlo track structure simulations for low-LET radiation such as electrons and γ-rays.

The chemical reactions are started from the spatially isolated entities, i.e. spurs. Primary spurs contain only small numbers of reactive ions and radicals [22]. The radius of an initial spur was estimated to be 1 nm, and the interspaces between spurs are several hundred nm for photon radiation and low-LET particle radiation. The spurs caused by photon radiation and/or low-LET particle radiation are sparsely distributed and unable to interact with each other. The initial reactive species caused in a spur react with water and each other, generate relatively stable species, and diffuse to a uniform distribution. The distance between spurs becomes shorter as the LET increases, and the spurs caused by high-LET radiation can overlap to form larger volumes, such as a blob or cylindrical volume, referred to as the core. The carbon-ion beam has a track structure consisting of the core region, which is formed by linear dense ionization caused by primary particles, and the penumbra region, which is branched ionization tracks formed by secondary electrons [24,25]. The Monte Carlo simulation was also used to estimate the yields of multiple reactive species caused by high-LET radiation [26,27].

Free radical generation on the track of heavy-ion beams

In early stage of therapeutic applications of heavy-ion beams, the direct action of heavy-ion beams based on their dense ionizing/exciting at the core was focused on. Free radicals directly formed on solid DNA and its constituents after heavy-ion beam irradiation were investigated using electron paramagnetic resonance

(EPR) spectroscopy [28–30]. These experiments were performed using a high dose, several kGy to several hundred kGy, and at low temperature, <100 K. Free radicals formed on the dry DNA samples by direct ionization of DNA or its constituents are few and unstable. However, in the cell nucleus, DNA is tightly packed by furling on histones, and only small amount of free water and hydration water on the DNA molecules could be existed. Therefore, direct actions on the DNA would be more important in such circumstance.

Indirect action and oxygen effects on the heavy-ion beams are of concern because of their altered biological effects. The effects of oxygen on the cell survival rate, i.e. oxygen enhancement ratio (OER), have been investigated from the early stage of particle beam employment, and an OER around 2 was obtained for 910-MeV helium-beams [31,32]. DNA strand breaks and repair in cells were investigated with or without DMSO, and DMSO exerted protective effects on the cell survival even after 960-MeV/n ^{235}U-beam [33] or 600-MeV/n iron-beam irradiation [34].

These reports demonstrated that water-derived initial reactive species, such as •OH, •H, and e_{aq}^-, are important for the biological effects of heavy-ion beams. The most reactive specie among ROS and/or other free radical species is •OH. Therefore, •OH has been considered the main player in the biological effects of ionizing radiation for past few decades. However, considering less water circumstances, such as tightly packed DNA in the nucleus and/or lipid in the cell membrane, contributions of •OH or other initial species to the biological effects may be not so high. Heavy-ion beams induced more clustered DNA damage, i.e. double-strand breaks, than photon radiation [35,36]. Milligan et al. [37] described that such clustered DNA damage is induced by clustering direct ionization rather than clustering •OH.

Detection/estimation of •OH

As described above, •OH was recognized as the major player in the biological effects of ionizing radiation. Therefore, how much •OH is generated and how •OH is distributed on the track of the heavy-ion beams are of interest.

Moritake et al. [38] measured carbon-ion beam-induced •OH by an EPR spin-trapping method using 5,5-dimethyl-1-pyrroline-*N*-oxide (DMPO) as the spin-trapping agent. They observed the generation of •OH and •H, i.e. DMPO-OH and DMPO-H, in the aqueous sample solution irradiated by carbon-ion beams. In addition, it was confirmed that these radicals are induced from water radiolysis because the deuterated radical adducts of DMPO, i.e. DMPO-OD and DMPO-D, were observed when deuterated water (D_2O) was irradiated. The yields of carbon-beam-induced •OH were LET-dependent and decreased with increasing LET.

Taguchi and Kojima [39] estimated the yield of •OH induced by carbon- or neon-beams in aqueous solution using another chemical reaction. An oxygen- or helium-saturated aqueous phenol (C_6H_5OH) solution was irradiated by carbon- or neon-beams, and the oxidized products of phenol, i.e. catechol, resorcinol, and hydroquinone, were analyzed using HPLC detected by absorption at 280 nm. For the identical ion, the yield of •OH increased as the specific energy of the ion increased. For specific energy, a lower yield of •OH was observed with a larger atomic number of the ion.

The yield of •OH induced by several different particles was estimated based on a super diffusion model calculation [40]. The yields of water-derived radicals, such as e_{aq}^-, •OH, •H, and hydrogen peroxide (H_2O_2), calculated by this super diffusion model were set up to approximate Fricke G-values, G(Fe^{3+}), which is well calibrated experimental value of the yield of Fe^{3+}in a microsecond. To estimate the yield of •OH in a nanosecond, the internal distances of supers caused along primary particles and those caused by secondary electrons, which are used in the super diffusion model calculation, were adjusted. They demonstrated the particle dependence of •OH yields, i.e. more for light particles, such as electrons, and less for heavy particles such as iron.

Radiation-induced •OH generated in irradiated sample solutions was again investigated by the EPR spin-trapping technique using DMPO as the spin-trapping agent [41]. The •OH adduct of DMPO, i.e. DMPO-OH, is unstable, and gradually decreases with a half-life of around 40–120 min at room temperature under aerobic conditions. Decay of DMPO-OH during and after irradiation must be corrected to quantify the net DMPO-OH yield using an iterative calculation [42]. Then, using a series of several concentrations (0.49–2778 mM) of DMPO solutions, DMPO-OH induced in each DMPO concentration was quantified and plotted versus the DMPO density (μm^{-1}), which was defined as the number of DMPO molecules aligned on the linear unit distance. The DMPO density is actually reciprocal of the intermolecular distance of DMPO molecules at a certain concentration. Since the ionizations are sequential events occurred on the track of photon, electron, or charged particles, the distribution of ionizations are not uniform in the 3-dimensional volume. Therefore, description of 1-dimensional density, i.e. the numbers of molecular

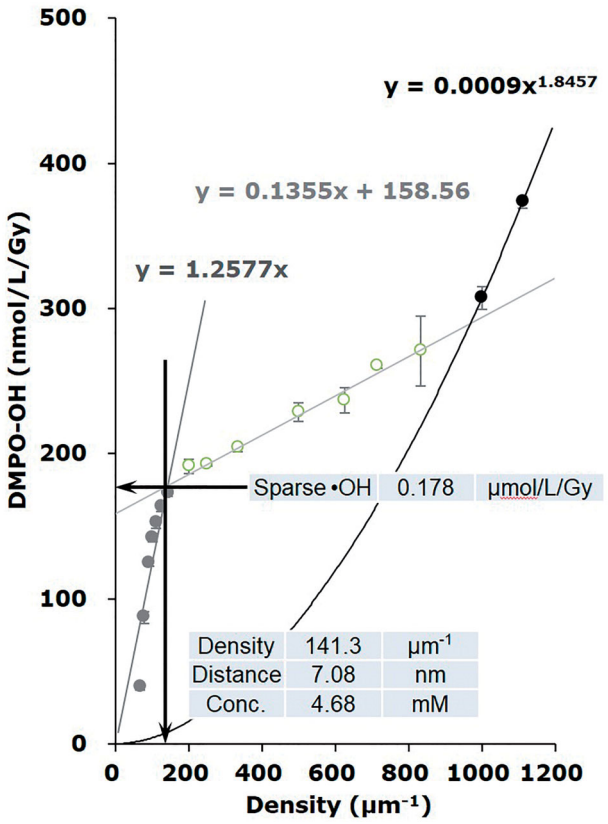

Figure 2. Typical 3-phase profile of the concentration of DMPO-OH plotted versus the density of DMPO observed by X-ray irradiation. The vertical down arrow through the inflection point of the 1st phase (solid gray circles) and 2nd phase (open circles) indicates the density of relatively sparse •OH generation, and the density was estimated to be 141.3 μm^{-1}, which was converted to 7.1 nm as the intermolecular distance and to 4.7 mM as the local concentration. The horizontal left arrow through the inflection point of the 1st phase and 2nd phase indicates the average yield of DMPO-OH in large sample volume. The 3rd phase (solid black circles) may continue to increase, but the end of 3rd phase was not observed in this experiment. The highest density of DMPO used was 1111 μm^{-1}, which corresponds to 0.9 nm as the molecular distance and 2278 mM as the concentration. The figure was partly modified from a previous report [46].

probes on the unit distance, was required to estimate density of radical distribution caused by the ionizations. The plot of DMPO-OH versus DMPO density exhibits a characteristic 3-phase profile (Figure 2).

When a series of DMPO solutions of different concentrations was irradiated by an identical dose, the amount of •OH detected, i.e. yield of DMPO-OH, linearly increased until the DMPO density matched the commensurate density of •OH generated in the sample. When the DMPO density exceeded the density of •OH generated in the sample solution, the yield of DMPO-OH became constant, and the inflection point of the 1st and 2nd phases appeared. The appearance of the 3rd phase reflects different •OH generation at a much higher density; however, the end of the 3rd phase was not observed. Two different localized densities of •OH generation were determined. The intermolecular distance of the lower •OH density was estimated as 4.3–6.6 nm from the inflection point of the 1st and 2nd phases, and that of the higher •OH density was estimated as 1 nm or shorter from the maximum DMPO density used in the experiment. These correspond to milli-molar level (relatively sparse) and molar level (markedly dense) generation. As the yields of DMPO-OH observed at the inflection point of the 1st and 2nd phases and at maximum DMPO density were both at micro-molar levels, the DMPO-OH generation, i.e. •OH generation, was a localized event on the radiation track.

The two different densities of localized •OH generation did not vary according to the LET of carbon-beams; however, the yields of sparse •OH, i.e. yield of DMPO-OH observed at the inflection point of 1st and 2nd phases, decreased with increasing LET [41,43]. On the other hand, the yield of DMPO-OH observed at the maximum DMPO density was not affected by LET. This suggests that the percentage of sparse •OH generation among the total •OH generation decreases with a higher LET, or that the percentage of dense •OH generation increases with a higher LET.

The two different densities of localized •OH generation were not dependent on the dose, dose rate, and/or energy of photons [44]. The half-dose experiment gave a half yield of DMPO-OH. Nearly identical 3-phase profiles were obtained in the experiments conducted with several different dose rates. The X-rays (E_{eff} = 80 keV) and γ-rays from ^{137}Cs (0.66 MeV) experiments also exhibited almost identical 3-phase profiles. In addition, 5 mM caffeine inhibited the sparse •OH generation, but the dense •OH generation and 3rd phase were unaffected.

The spin-trapping efficiency of DMPO for γ-ray induced •OH was reported to be 35% [45]. In this experiment, the radiation-induced •OH and •H in water were used as standards for estimating the spin-trapping efficiency of DMPO and POBN because their distribution was considered to be almost uniform three-dimensionally. Several concentrations of DMPO solutions were irradiated by 136-Gy γ-rays and DMPO-OH induced in the samples was measured. The maximum concentration of DMPO-OH measured at the plateau was 14.2 μM, which was 35% of the expected yield of •OH, 40 μM, calculated from the G-value. The maximum concentration of DMPO solutions used in their experiment was 440 mM; therefore, this observation reflects only the sparse component of •OH generation.

The highest DMPO concentration used in our previous reports for estimating the density of •OH generation was 2278 mM [46]. The yield of DMPO-OH was 0.373 ± 0.004 μmol/L/Gy when the 2278 mM DMPO solution was irradiated by X-rays. The yield of •OH expected from the initial G-value of •OH of 5.6, which is the yield of •OH at the physicochemical stage ($\leq 10^{-11}$ s) [47], was 0.581 μmol/L/Gy. The detection efficiency was therefore greater than 64%. When the primary G-value of •OH of 2.7, which is the yield of •OH at the chemical stage ($\geq 10^{-7}$ s) [48] was used, the expected yield of •OH was 0.280 μmol/L/Gy, less than our experimental DMPO-OH yield. The EPR spin-trapping method can scavenge •OH, probably the initial yield, during its markedly short lifetime, enabling the collection of information about momentary •OH generation. Therefore, the EPR spin-trapping method cannot analyze the time course of initial to primary reactions of water radiolysis, unlike pulse radiolysis techniques.

The molecular volumes of a single DMPO molecule and single water molecule were calculated as 0.19 nm^3 and 0.03 nm^3, respectively. At a concentration of 2278 mM, one DMPO molecule occupies 0.73 nm^3. Only 18 water molecules can fill the remaining 0.54 nm^3. In other words, one DMPO is monitoring only 18 vicinal water molecules. When one of the 18 water molecule is ionized/excited to give •OH, the trapping efficiency of the DMPO for this initial •OH molecule may be more than 64%, even though the second one was not detected.

A compound added to the reaction system has the opportunity to trap •OH because •OH can react with most molecules with low selectivity due to their high reactivity, although •OH exhibits slight selectivity [42]. Sugars have less •OH canceling ability compare to caffeine, but caffeine has higher •OH canceling ability than sugars [42]. The addition of 5 mM caffeine to DMPO sample solution as a •OH scavenger can inhibit the relatively sparse •OH generated at a comparable concentration, whereas the markedly dense •OH generation was not altered [44,46]. However, phosphates added as a buffer at 100 mM in the DMPO sample solution had almost no effect on scavenging •OH [49]. Indeed, in Matsumoto et al. [41] and Ueno et al. [46], 100 mM phosphate buffer was used, and in Ogawa et al. [44], pure waste was used as the solvent of DMPO, but the results were similar.

Detection of H_2O_2

The yield of H_2O_2 expected from the primary G-value of H_2O_2 of 0.7 [48] was 0.073 μmol/L/Gy. However, a larger yield of H_2O_2 was experimentally observed as 0.26 ± 0.01 μmol/L/Gy in an X-ray-irradiated water sample [43]. For 20 keV/μm carbon-ion beams, the yield of H_2O_2 was 0.20 ± 0.01 μmol/L/Gy. The yield of H_2O_2 slightly decreased with increasing LET, and 0.17 ± 0.01 μmol/L/Gy was observed for >100 keV/μm carbon-ion beams. Experimentally observed H_2O_2 yields were measured several hours to days after irradiation. H_2O_2 generation in aerobic conditions is associated with oxygen consumption [43,50]. At the beginning, hydroperoxyl radials ($HO_2^•$) are generated by the reaction of a •H and oxygen (O_2) (Equation (1)), or by the reaction of excited water (H_2O^*) and O_2 (Equation (2)). Then, H_2O_2 is generated by the reaction of 2 $HO_2^•$ (Equation (3)).

$$•H + O_2 \rightarrow HO_2^• \quad (1)$$

$$H_2O^* + O_2 \rightarrow •OH + HO_2^• \quad (2)$$

$$HO_2^• + HO_2^• \rightarrow H_2O_2 + O_2 \quad (3)$$

The oxygen consumption was also LET-dependent, and decreased with increasing LET. The amount of oxygen consumption was 0.41 ± 0.04, 0.39 ± 0.15, and 0.05 ± 0.13 μmol/L/Gy for X-rays, 20 keV/μm carbon-ion beams, and >100 keV/μm carbon-ion beams, respectively. The ratios of H_2O_2 generation per oxygen consumption were 0.63, 0.51, and 3.40 for X-ray, 20 keV/μm carbon-ion beams, and >100 keV/μm carbon-ion beam, respectively. Therefore, oxygen-independent H_2O_2 generation increased with increasing LET.

Oxygen-independent H_2O_2 generation is through the reaction of 2 •OH (Equation (4)). However, the 2 •OH must be close to react.

$$•OH + •OH \rightarrow H_2O_2 \quad (4)$$

Two different localized densities of •OH generation, milli-molar level and molar level generation, were previously reported [41]. In the molar level •OH environment, the intermolecular distance of two •OH is less than 1 nm, and they are able to react and directly generate H_2O_2. If •OH is densely generated, a highly concentrated H_2O_2 cluster may form. In such conditions, further reactions of the H_2O_2 and nearby •OH (Equation (5)) may produce $HO_2^•$ and another H_2O_2 can be generated by Equation (3).

$$H_2O_2 + •OH \rightarrow H_2O + HO_2^• \quad (5)$$

In practice, both oxygen-dependent and -independent H_2O_2 were produced simultaneously in the reaction mixture under an aerobic condition. The reaction converged on relatively stable H_2O_2 and H_2O_2 remained for a long time in water.

4-Hydroxyl-2,2,6,6-tetramethylpiperidine-*N*-oxyl (TEMPOL), which is used as a redox-sensitive molecular

probe in magnetic resonance fields, is a stable nitroxyl radical solely in water. A nitroxyl radical (>N-O•) can be one-electron oxidized by •OH and/or $HO_2^•$ to give the oxioamonium cation (>N^+=O), and subsequently two-electron reduced by receiving hydride from a hydride donor, such as NAD(P)H, to be hydroxylamine (>N-OH). A nitroxyl radical can be one-electron reduced directly by a relatively strong reductant such as ascorbic acid.

When the water solution of TEMPOL was irradiated with relatively high-dose X-rays or carbon-ion beams, the EPR signal of TEMPOL decreased even though hydrogen and hydride donors were absent in the solution [43,50]. As this hydrogen or hydride donor-independent reduction of TEMPOL was partly suppressed by catalase, the generation of H_2O_2 in water is probably related to this reaction [50]. Another type of nitroxyl radical, 3-carbamoyl-2,2,5,5-tetramethylpyrrolidine-*N*-oxyl (carbamoyl-PROXYL) also demonstrated similar reduction [46]. Although the detailed mechanism underlying this hydrogen or hydride donor-independent reduction of nitroxyl radicals is unclear, the combination of a highly concentrated H_2O_2 environment and an oxidative stimulation to trigger the reaction may be related to the decrease in nitroxyl radicals [46].

In the high-density •OH environment described above, •OH can react and directly make H_2O_2, and then possibly form a high-density H_2O_2 cluster. The distance between such clusters was estimated using nitroxyl radicals, TEMPOL, and carbamoyl-PROXYL, as are dox probe for detecting highly concentrated H_2O_2 [46]. The method for density estimation of •OH was modified and the internal distance of X-ray-induced H_2O_2 clusters was estimated [46]. A series (1.66–1248 μM) of the nitroxyl radical water solutions was used to detect highly concentrated H_2O_2 instead of DMPO. EPR signal loss of nitroxyl radicals was plotted versus the density of the nitroxyl probe. As a result, the internal distance of the high-concentration H_2O_2 clusters was estimated as 40–47 nm from the inflection point of the plot (Figure 3). This study suggested that irradiating an aqueous solution with ionizing radiation creates a localized highly concentrated H_2O_2 environment scattered and separated by 40–47 nm.

This reaction using a nitroxyl radial as a redox probe was visualized by T_1-weightd MRI [50]. In an aqueous gelatin volume sample, the distribution of highly concentrated H_2O_2 clusters exhibited a relatively flat profile

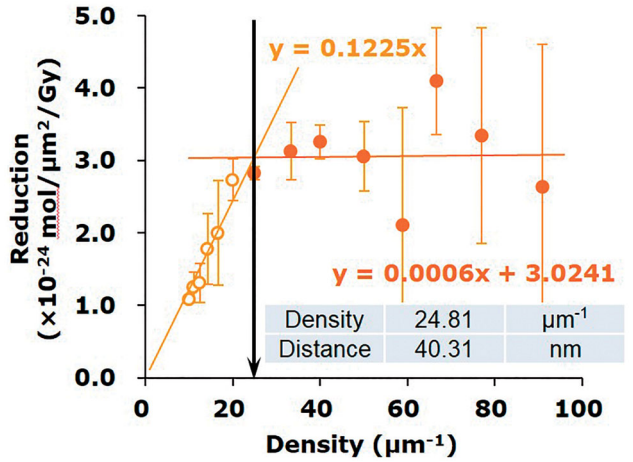

Figure 3. The 2-phase profile observed by plotting high-concentration H_2O_2-induced TEMPOL reduction versus the density of TEMPOL in the sample solution. The vertical down arrow through the inflection point indicates a density of the high-concentration H_2O_2 clusters, and the density was estimated to be 24.8 μm^{-1}, which was converted to 40.3 nm as the inter-space distance of the clusters. The figure was partly modified from a previous report [46].

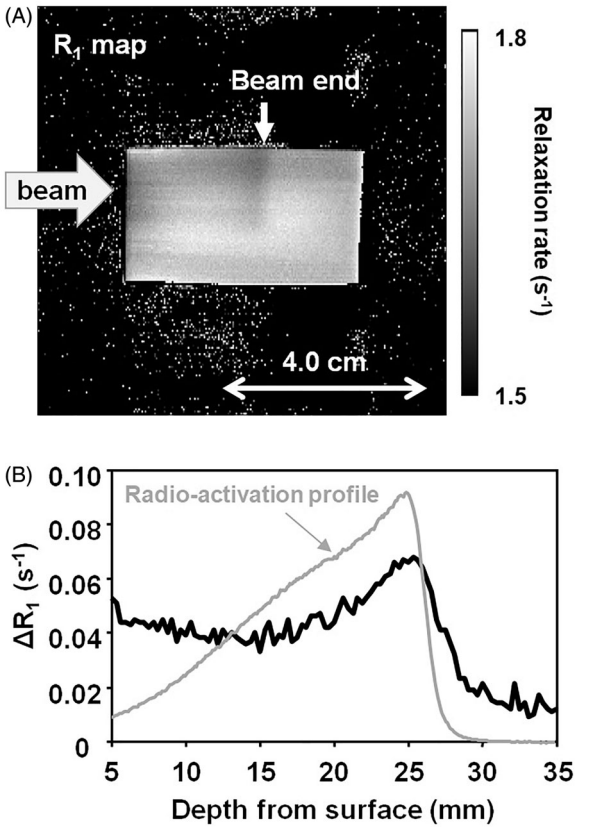

Figure 4. Visualized distribution of high-concentration H_2O_2 clusters in a gelatin sample. (A) R_1 (= $1/T_1$) map of the gelatin sample containing 2 mM TEMPOL irradiated by 200-Gy carbon-ion beams at the surface. Matrix size = 128 × 128, field of view = 80 × 80 mm, slice thickness = 2 mm. The upper half of surface side was slightly darkened due to the reduction of TEMPOL. (B) Profile of percentage decay of MR signal (solid black line) in the irradiated part of the sample. The radio-activation profile in the gelatin measured at the same time was overlapped (gray line). The figure was partly modified from our previous report [50].

from the surface to near the beam end, except for a small peak at the beam end (Figure 4).

H_2O_2 at a high concentration is a strong oxidant. The separation distance of 40–47 nm of H_2O_2 clusters may be related to the frequency of oxidation induced by the highly concentrated H_2O_2 induced by photon radiation in hypoxic biological environments. In hypoxic conditions, like *in vivo*, only clustered H_2O_2 generation may be available because clustered •OH, i.e. markedly dense •OH, may be the only source of H_2O_2 generation. Ion-beams may generate H_2O_2 clusters separated by a shorter distance or connected/overlapped at the core region. Therefore, oxidation reactions induced by the highly concentrated H_2O_2 of ion-beams will be denser.

Detection of superoxide($O_2^{\bullet-}$)/$HO_2^{\bullet}$ or related reactions

$HO_2^{\bullet}/O_2^{\bullet-}$ production induced by sulfur-ion beam (2.7 GeV/nucleon) in water was measured using the pulse radiolysis technique with absorption at 260 nm [51]. A higher yield of $O_2^{\bullet-}$ in aerated water than in de-aerated water was reported.

Detection of radiation-induced $HO_2^{\bullet}/O_2^{\bullet-}$ production by EPR spin-trapping is difficult. As describe above, $HO_2^{\bullet}$ was generated by the reaction of •H and O_2 (Equation (1)) in aerobic conditions. The $HO_2^{\bullet}$ is equilibrated with $O_2^{\bullet-}$ in aqueous solutions (Equation (6)).

$$HO_2^{\bullet} \rightleftarrows O_2^{\bullet-} + H^+ \quad (6)$$

In hypoxic conditions, $HO_2^{\bullet}$ is generated from •OH through Equations (4) and (5). The constituents of $HO_2^{\bullet}/O_2^{\bullet-}$ production, i.e. •H and •OH, were spin-trapped and canceled when a sufficient amount of spin-trapping agent was added.

The reaction of $HO_2^{\bullet}/O_2^{\bullet-}$ with a nitroxyl radical was able to be measured using an EPR redox probing method such as total oxidation [43,52]. Highly oxidative ROS, such as •OH and $HO_2^{\bullet}$, can oxidize biological molecules. The amount of total oxidation can be compared with the amount of oxidative free radicals. A nitroxyl radical can be one-electron oxidized to an oxoamonium cation by •OH and $HO_2^{\bullet}$. In the presence of glutathione, the oxoamonium cation can be reduced to hydroxylamine by receiving a hydrogen atom from glutathione or form a stable compound with glutathione. Therefore, the amount of total oxidation can be measured by the amount of GSH-dependent reduction of nitroxyl radicals. The amount of total oxidation reactions was estimated as 3 μmol/L/Gy for X-rays.

Total oxidation caused by carbon-ion beams was lower than that by X-rays at the same dose (Figure 5). For carbon-ion beams, the amount of total oxidation

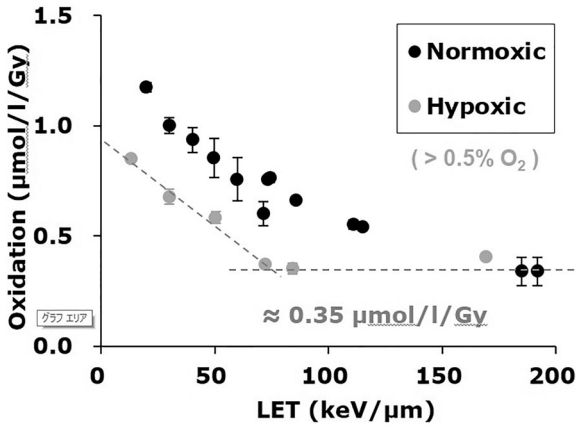

Figure 5. Carbon-ion beam-induced total oxidation reaction. Black and gray marks indicate the results of aerobic and hypoxic experiments, respectively. Marks and error bars indicate the average ± SD of three experiments. A dotted line in the figure indicates the level of 0.35 μmol/L/Gy, which was considered to be from •OH. The difference between aerobic and hypoxic experiments was the contribution of $HO_2^{\bullet}$. The figure was partly modified from our previous report [43].

decreased with increasing LET when an identical dose was administered [43,52]. When the same experiment was performed under hypoxic conditions, the amount of total oxidation decreased. However, the amount of total oxidation under hypoxic conditions was not affected by a high-LET (>150 keV/μm). The lowest level of total oxidation was 0.35 μmol/L/Gy, which can be considered a result of •OH.

This reaction was also visualized by MRI to observe the oxidative ROS distribution in an intact volume gelatin sample [43]. A cylindrical gelatin sample was irradiated by carbon-ion beams (Figure 6). The lower half of the sample was shaded by a brass filter. After irradiation, the sample was scanned by 7-T MRI using a T_1-weighted sequence. In a vertical 2 mm slice of the sample, the dark part is the irradiated part. The profile of reduction of TEMPOL extracted from the MR image was almost flat from the surface to near the beam end, with a slight peak at the beam end.

Generation of free radicals in lipids

Cells have a complicated structure with a lipid bilayer membrane floating in water. Free radical generation in the water phase have been well investigated. However, there are few reports of heavy-ion induced free radicals in lipids. Experimental reports of the quantification of lipid-derived free radicals are limited due to the absence of a good quantification method. Only direct lipid peroxidation induced by heavy-ion in liposomes and lipoproteins has been reported [53,54].

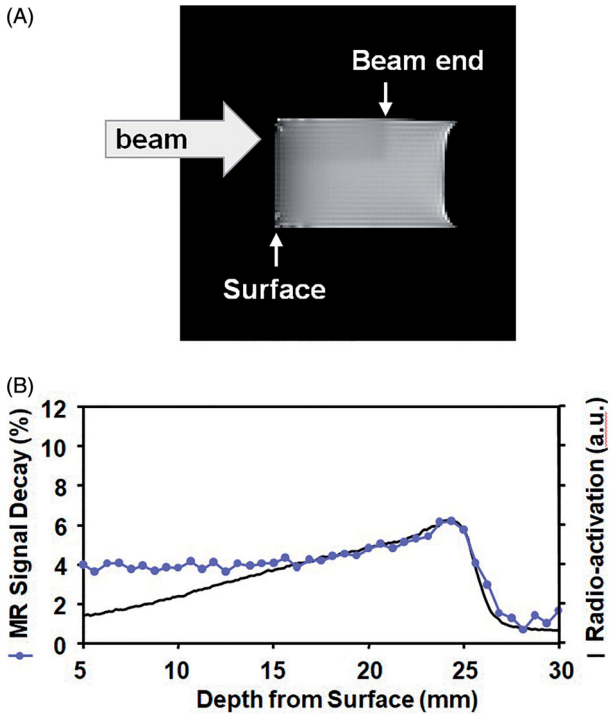

Figure 6. Visualized distribution of oxidative ROS in a gelatin sample. (A) T_1-weightedimage of the gelatin sample containing 2 mM TEMPOL and 4 mM GSH irradiated by 200-Gy carbon-ion beams at the surface. Matrix size = 128 × 128, field of view = 80 × 80 mm, slice thickness = 2 mm. The upper half of the surface side was slight darkened due to the reduction of TEMPOL. (B) Profile of percentage decay of MR signal (solid circle with line) in the irradiated part of the sample. The radio-activation profile in the gelatin measured at the same time was overlapped (solid black line). The figure was partly modified from our previous report [52].

Redox reactions caused by different qualities of radiation, i.e. X-rays or carbon-ion beams (LET = 13 keV/μm), in several solvents were observed and compared [55]. Using 2,2-diphehyl-1-picrylhydrazyl radical (DPPH•) and its water-solubilized preparation of DPPH•, which is the complexation of DPPH• with β-cyclodextrin [56,57], as a redox probe, the dose dependency of free radical decay in the irradiated water, methanol, acetonitrile, and isopropyl myristate was observed by monitoring the absorption of DPPH• at 527, 516, 519, and 517 nm, respectively. DPPH• linearly decayed as the dose increased. The decay slopes of DPPH• caused by X-rays and carbon-ion beams were similar in water, methanol, and acetonitrile; however, X-ray-induced DPPH• decay in isopropyl myristate was lower than that induced by carbon-ion beams. Free radical generation in lipids may differ with the quality of radiation.

Conclusion

Carbon-ion beam therapy, a modern charged particle radiation therapy, is becoming increasingly common option of medical treatment for cancer and/or other diseases. Differences in ionization and ROS generation properties between photon and charged particle radiation on its track structure would lead to differences in the biological effects. Localized ionization in irradiated water and subsequent generation of reactive species, which were estimated by simulations and pulse radiolysis experiments, were chemically detected by EPR spin-trapping and spin-probing techniques, and their accuracy was confirmed. There were differences between methods, but the results were consistent. Such localization of reactive species, especially •OH, may produce an unknown chemical environment such as highly concentrated H_2O_2. The local density of initial/primary reactive species and the oxygen concentration can decide the course of ROS generation reactions. In addition, little is known about radiation-induced free radical generation in lipidic conditions. Although free radical generation in lipids may differ with the quality of radiation, the radio-chemical and radio-biological effects in lipids remain unclear.

Acknowledgements

The authors are grateful to the staff of the HIMAC for their help in irradiating samples by carbon-ion beams.

Disclosure statement

No potential conflict of interest was reported by the author(s).

Funding

The studies introduced in this review were partly supported by JSPS KAKENHI; Grant Numbers 23591853 (K. M.), 18K07695 (K. M.), 18K07739 (M. U.), and 18K06620 (I. N.).

References

[1] Dale WM. The effect of X-rays on the conjugated protein d-amino-acid oxidase. Biochem J. 1942;36(1-2):80–85.
[2] Dale WM, Davies JV, Meredith WJ. Observations on the indirect action of ionizing radiation on aqueous solutions. Biochem J. 1946;40(3):xxxviii.
[3] Barron ESG, Dickman S, Muntz JA, et al. Studies on the mechanism of action of ionizing radiations; inhibition of enzymes by X-rays. J Gen Physiol. 1949;32(4):537–552.
[4] Goodhead DT. Mechanisms for the biological effectiveness of high-LET radiations. JRR. 1999;40(Suppl):1–13.
[5] Chapman JD, Doern SD, Reuvers AP, et al. Radioprotection by DMSO of mammalian cells

exposed to X-rays and to heavy charged-particle beams. Radiat Environ Biophys. 1979;16(1):29–41.
[6] Roots R, Chatterjee A, Chang P, et al. Characterization of hydroxyl radical-induced damage after sparsely and densely ionizing irradiation. Int J Radiat Biol Relat Stud Phys Chem Med. 1985;47(2):157–166.
[7] Raju MR, Amols HI, Carpenter SG. A combination of sensitizers with high LET radiations. Br J Cancer. 1978; 37(Suppl. III):189–193.
[8] Hirayama R, Furusawa Y, Fukawa T, et al. Repair kinetics of DNA-DSB induced by X-rays or carbon ions under oxic and hypoxic conditions. J Radiat Res. 2005; 46(3):325–332.
[9] Tsujii H, Mizoe J, Kamada T, et al. Clinical results of carbon ion radiotherapy at NIRS. JRR. 2007;48(Suppl. A):A1–A13.
[10] Web site of National Institutes for Quantum and Radiological Science and Technology, Chiba, Japan., Quantum Medical Science Directorate, Dept. of Charged Particle Therapy Research. [cited 2020 Oct 29]. Available from: https://www.qst.go.jp/site/nirs-english/1361.html.
[11] Web site of National Institutes for Quantum and Radiological Science and Technology, Chiba, Japan., Quantum Medical Science Directorate, Heavy Ion Radiotherapy. [cited 2020 Oct 29]. Available from: https://www.qst.go.jp/site/nirs-english/40056.html.
[12] PDF brochure of Gunma University Heavy Ion Medical Center. [cited 2020 Oct 30]. Available from: https://heavy-ion.showa.gunma-u.ac.jp/en/pdf/panf001_en.pdf.
[13] PDF brochure of SAGA HIMAT (SAGA Heavy-Ion Medical Accelerator in Tosu). [cited 2020 Oct 30]. Available from: https://www.saga-himat.jp/library/pdf/A-english.pdf.
[14] Web site of "i-ROCK Facility,"i-ROCK (Ion-beam Radiation Oncology Center in Kanagawa). [cited 2020 Oct 30]. Available from: http://kcch.kanagawa-pho.jp/i-rock/english/facility/index.html.
[15] Web site of "Greetings and department introduction,"Osaka HIMAK at Osaka Heavy Ion Therapy Center. [cited 2020 Oct 30]. Available from: https://www.osaka-himak.or.jp/en/about/message/.
[16] Web site of "Greeting,"Hyogo Ion BeamMedical Center. [cited 2020 Oct 30]. Available from: https://www.hibmc.shingu.hyogo.jp/lang/english.html.
[17] Web site of National Institutes for Quantum and Radiological Science and Technology, Chiba, Japan., Quantum Medical Science Directorate, Dept. of Accelerator and Medical Physics. [cited 2020 Oct 29]. Available from: https://www.qst.go.jp/site/nirs-english/1359.html.
[18] Kamada T. Clinical evidence of particle beam therapy (carbon). Int J Clin Oncol. 2012;17(2):85–88.
[19] Noda K. Beam delivery method for carbon-ion radiotherapy with the heavy-ion medical accelerator in chiba. Int J Part Ther. 2016;2(4):481–489.
[20] Ohno T. Particle radiotherapy with carbon ion beams. Epma J. 2013;4(1):9.
[21] Takahashi W, Mori S, Nakajima M, et al. Carbon-ion scanning lung treatment planning with respiratory-gated phase-controlled rescanning: simulation study using 4-dimensional CT data. RadiatOncol. 2014;9:238.
[22] Samuel AH. Theory of radiation chemistry. V. Generalized spur diffusion model. J Phys Chem. 1962; 66(2):242–245.
[23] Mozumder A, Magee JL. Model of tracks of ionizing radiations for radical reaction mechanism. Radiat Res. 1966;28(2):203–214.
[24] Muroya Y, Plante I, Azzam EI, et al. High-LET ion radiolysis of water: visualization of the formation and evolution of ion tracks and relevance to the radiation-induced bystander effect. Radiat Res. 2006;165(4): 485–491.
[25] Conte V, Selva A, Colautti P. Track structure of carbon ion: new measurements and simulations. Radiat Phys Chem. 2020;168:108576.
[26] Meesungnoen J, Jay-Gerin JP. High-LET radiolysis of liquid water with $^{1}H^{+}$, $^{4}He^{2+}$, $^{12}C^{6+}$, and $^{20}Ne^{9+}$ ions: Effects of multiple ionization. J Phys Chem A. 2005; 109(29):6406–6419.
[27] Yamashita S, Katsumura Y, Lin M, et al. Water radiolysis with heavy ions of energies up to 28 GeV. 3. Measurement of G(MV*+) in deaerated methyl viologen solutions containing various concentrations of sodium for mate and Monte Carlo simulation. Radiat Res. 2008;170(4):521–533.
[28] Hüttermann J, Schaefer A, Kraft G. Free radicals induced in solid DNA by heavy ion bombardment. Adv Space Res. 1989;9(10):35–44.
[29] Schaefer A, Huttermann J, Kraft G. Direct radiation action of heavy ions on DNA as studied by ESR-spectroscopy. Adv Space Res. 1992;12(2-3):45–49.
[30] Becker D, Razskazovskii Y, Callaghan MU, et al. Electron spin resonance of DNA irradiated with a heavy-ion beam ($^{16}O^{8+}$): evidence for damage to the deoxyribose phosphate backbone. Radiat Res. 1996; 146(4):361–368.
[31] Raju MR, Gnanapurani M, Madhvanath U, et al. Relative biologic effectiveness and oxygen enhancement ratio at various depths of a 910-MeV helium ion beam. Acta Radiol Ther Phys Biol. 1971;10(3):353–357.
[32] Raju MR, Gnanapurani M, Martins B, et al. Measurement of OER and RBE of a 910 MeV helium ion beam, using cultured cells (T-1). Radiology. 1972; 102(2):425–428.
[33] Yang TC, Tobias CA. Neoplastic cell transformation by energetic heavy ions and its modification with chemical agents. Adv Space Res. 1984;4(10):207–218.
[34] Yang TC, Mei M, George KA, et al. DNA damage and repair in oncogenic transformation by heavy ion radiation. Adv Space Res. 1996;18(1-2):149–158.
[35] Brenner DJ, Ward JF. Constraints on energy deposition and target size of multiply damaged sites associated with DNA double-strand breaks. Int J Radiat Biol. 1992;61(6):737–748.
[36] Terato H, Ide H. Clustered DNA damage induced by heavy ion particles. Biol Sci Space. 2004;18(4):206–215.
[37] Milligan JR, Aguilera JA, Paglinawan RA, Ward JF, et al. DNA strand break yields after post-high LET irradiation incubation with endonuclease-III and evidence for hydroxyl radical clustering. Int J Radiat Biol. 2001; 77(2):155–164.

[38] Moritake T, Tsuboi K, Anzai K, et al. ESR spin trapping of hydroxyl radicals in aqueous solution irradiated with high-LET carbon-ion beams. Radiat Res. 2003; 159(5):670–675.
[39] Taguchi M, Kojima T. Yield of OH radicals in water under high-density energy deposition by heavy-ion irradiation. Radiat Res. 2005;163(4):455–461.
[40] Yamaguchi H, Uchihori Y, Yasuda N, et al. Estimation of yields of OH radicals in water irradiated by ionizing radiation. J Radiat Res. 2005;46(3):333–341.
[41] Matsumoto K, Ueno M, Nakanishi I, et al. Density of hydroxyl radicals generated in an aqueous solution by irradiating carbon-ion beam. Chem Pharm Bull (Tokyo)). 2015;63(3):195–199.
[42] Ueno M, Nakanishi I, Matsumoto K. Method for assessing X-ray-induced hydroxyl radical scavenging activity of biological compounds/materials. J ClinBiochemNutr. 2013;52(2):95–100.
[43] Matsumoto K, Nyui M, Ueno M, et al. A quantitative analysis of carbon-ion beam-induced reactive oxygen species and redox reactions. J Clin Biochem Nutr. 2019;65(1):1–7.
[44] Ogawa Y, Sekine-Suzuki E, Ueno M, et al. Localized hydroxyl radical generation at mmol/L and mol/L levels in water by photon irradiation. J Clin Biochem Nutr. 2018;63(2):97–101.
[45] Carmichael AJ, Makino K, Riesz P. Quantitative aspects of ESR and spin trapping of hydroxyl radicals and hydrogen atoms in gamma-irradiated aqueous solutions. Radiat Res. 1984;100(2):222–234.
[46] Ueno M, Nakanishi I, Matsumoto K. Generation of localized highly concentrated hydrogen peroxide clusters in water by X-rays. Free Radic Res. 2020;54(5):360–372.
[47] LaVerne JA. OH radicals and oxidizing products in the gamma radiolysis of water. Radiat Res. 2000;153(2): 196–200.
[48] Baldacchino G, Brun E, Denden I, et al. Importance of radiolytic reactions during high-LET irradiation modalities: LET effect, role of O_2 and radiosensitization by nanoparticles. Cancer Na. 2019;10(1):3.
[49] Matsumoto K, Ogawa Y, Kamibayashi M, et al. Assessment of redox status in commercial bottled mineral water. J Clin Nutr Food Sci. 2018;1:29–34.
[50] Matsumoto K, Aoki I, Nakanishi I, et al. Distribution of hydrogen peroxide-dependent reaction in a gelatin sample irradiated by carbon ion beam. Magn Reson Med Sci. 2010;9(3):131–140.
[51] Baldacchino G, Le Parc D, Hickel B, et al. Direct observation of HO_2/O_2^- free radical generated in water by a high-linear energy transfer pulsed heavy-ion beam. Radiat Res. 1998;149(2):128–133.
[52] Matsumoto K, Nagata K, Yamamoto H, et al. Visualization of free radical reactions in an aqueous sample irradiated by 290 MeV carbon beam. Magn Reson Med. 2009;61(5):1033–1039.
[53] Ziegler C, Bonnefont-Rousselot D, Delacroix S, et al. Effectiveness of protons and argon ions in initiating lipid peroxidation in low-density lipoproteins. Radiat Res. 1998;150(4):483–487.
[54] Ziegler C, Wessels JM. Investigation of lipid peroxidation in liposomes induced by heavy ion irradiation. Radiat Environ Biophys. 1998;37(2):95–100.
[55] Nakanishi I, Yamashita S, Shimokawa T, et al. Analysis of redox states of protic and aprotic solutions irradiated by low linear energy transfer carbon-ion beams using a 2,2-diphenyl-1-picrylhydrazyl radical. Org Biomol Chem. 2018;16(8):1272–1276.
[56] Nakanishi I, Ohkubo K, Kamibayashi M, et al. Reactivity of 2,2-dipheniyl-1-picrylhydrazyl solubilized in water by β-cyclodextrin and its methylated derivative. Chemistry Select. 2016;1:3367–3370.
[57] Nakanishi I, Ohkubo K, Imai K, et al. Solubilisation of a 2,2-diphenyl-1-picrylhydrazyl radical in water by β-cyclodextrin to evaluate the radical-scavenging activity of antioxidants in aqueous media. Chem Commun (Camb). 2015;51(39):8311–8314.